Astronomy & Astrophysics

VLT spectroscopy of globular cluster systems[*]

II. Spectroscopic ages, metallicities, and [α/Fe] ratios of globular clusters in early-type galaxies

T. H. Puzia[1,2,**], M. Kissler-Patig[3], D. Thomas[4,5], C. Maraston[4,5],
R. P. Saglia[4], R. Bender[2,4], P. Goudfrooij[1], and M. Hempel[3]

[1] Space Telescope Science Institute, 3700 San Martin Drive, Baltimore, MD 21218, USA
e-mail: [tpuzia;goudfroo]@stsci.edu
[2] Sternwarte der Ludwig-Maximilians-Universität, Scheinerstr. 1, 81679 München, Germany
[3] European Southern Observatory, 85749 Garching bei München, Germany
e-mail: [mkissler;hempel]@eso.org
[4] Max-Planck-Institut für extraterrestrische Physik, Giessenbachstrasse, 85748 Garching bei München, Germany
e-mail: [bender;saglia]@mpe.mpg.de
[5] University of Oxford, Astrophysics, Keble Road, Oxford, OX1 3RH, UK
e-mail: [dthomas;maraston]@astro.ox.ac.uk

Abstract. An analysis of ages, metallicities, and [α/Fe] ratios of globular cluster systems in early-type galaxies is presented, based on Lick index measurements summarized in Puzia et al. (2004, A&A, 415, 123, Paper I of this series). In the light of calibration and measurement uncertainties, age-metallicity degeneracy, and the relative dynamic range of Lick indices, as well as systematics introduced by abundance ratio variations (in particular variations of [α/Fe] ratios), we find that the most reliable age indicator for our dataset is a combination of the Lick Balmer-line indices $H\gamma_A$, $H\beta$, and $H\delta_A$. [MgFe]′ is used as a spectroscopic metallicity indicator which is least affected by [α/Fe] variations. We introduce an interpolation routine to simultaneously derive ages, metallicities, and [α/Fe] ratios from diagnostic grids constructed from Lick indices. From a comparison of high-quality data with SSP model predictions, we find that ∼2/3 of the globular clusters in early-type galaxies are older than 10 Gyr, up to 1/3 have ages in the range ∼5−10 Gyr, and only a few cluster are younger than ∼5 Gyr. Our sample of globular clusters covers metallicities from [Z/H] ≈ −1.3 up to ∼0.5 dex. We find that metal-rich globular clusters show on average a smaller mean age and a larger age scatter than their metal-poor counterparts. [α/Fe] diagnostic plots show that globular cluster systems in early-type galaxies have super-solar α/Fe abundance ratios with a mean [α/Fe] = 0.47 ± 0.06 dex and a dispersion of ∼0.3 dex. We find evidence for a correlation between [α/Fe] and metallicity, in the sense that more metal-rich clusters exhibit lower α-element enhancements. A discussion of systematics related to the Lick index system shows that the method suffers to some extent from uncertainties due to unknown horizontal branch morphologies at high metallicities. However, these systematics still allow us to make good qualitative statements. A detailed investigation of indices as a function of data quality reveals that the scatter in Balmer index values decreases for higher-quality data. In particular, extremely low Balmer index values that are lower than any SSP model prediction tend to disappear. Furthermore, we find that observed photometric colors are in good agreement with computed SSP colors using ages and metallicities as derived from the spectroscopic line indices.

Key words. galaxies: star clusters – galaxies: general

1. Introduction

Two prominent models of early-type galaxy formation are lively discussed in the literature. In the *monolithic-collapse* scenario (Tinsley 1972; Larson 1975; Silk 1977;

Arimoto & Yoshii 1987, etc.) the majority of stars in early-type galaxies forms early, at redshifts $z \gtrsim 2$. Empirical scaling laws, such as the fundamental plane, the Mg–σ relation, and the [α/Fe]-σ relation support such an early formation epoch (Bower et al. 1992; Bender 1996; Bender et al. 1996; Treu et al. 1999; Kuntschner 2000; Trager et al. 2000a,b; Thomas et al. 2005; Peebles 2003). On the other hand, the *hierarchical merging* picture (White & Rees 1978; Kauffmann et al. 1993; Baugh et al. 1998; Cole et al. 2000; Somerville et al. 2001) sees

---

early-type galaxies as the result of multiple merging and accretion events of smaller units over an extended period of time until the very recent past. In this way a significant fraction of stars is formed below a redshift of unity. Observed ongoing mergers and accretion events (e.g. Whitmore & Schweizer 1995; Ibata et al. 1995; Koo et al. 1996) and the existence of kinematically decoupled cores (Franx & Illingworth 1988; Bender 1988; Jedrzejewski & Schechter 1988; Surma & Bender 1995; Davies et al. 2001) are clearly enforcing arguments for this scenario.

These models describe two antipodal paradigms of galaxy formation. The quantification of their importance as a function of redshift, environment, and galaxy morphology is necessary to provide detailed insight in galaxy formation and assembly. A major difference between the two pictures are the different star-formation histories of early-type galaxies. While in the hierarchical picture most massive galaxies are thought to experience long assembly time scales, the monolithic collapse scenario predicts very early and short bursts of star formation. Clearly, the predicted star-formation histories stand in marked contrast and are an important piece of evidence to differentiate between these two models.

However, to recover star-formation histories, one ideally has to resolve the underlying stellar populations which build up a galaxy. Only a few early-type systems are close enough so that their halos can be resolved into single stars (e.g. in M 32: Grillmair et al. 1996, NGC 3115: Elson 1997, NGC 5128: Harris & Harris 2002, NGC 3379: Gregg et al. 2004). Most photometric and spectroscopic studies of the unresolved diffuse light are hampered by the mix of ages, metallicities, and abundance ratios in the stellar populations (e.g. Maraston & Thomas 2000). In combination with the well-known age-metallicity degeneracy (Faber 1972; O'Connell 1976; Worthey 1994), it is extremely difficult to disentangle even the different major stellar populations from studies of the diffuse light only, let alone to reconstruct a detailed star formation history.

1.1. Globular cluster systems as diagnostics of star-formation histories

Globular cluster systems are very useful tools to study star formation histories of galaxies. Several arguments support the hypothesis that globular clusters trace major star-formation events in galaxies. (1) The formation of massive star clusters, which are likely to survive a Hubble time as globular clusters, is observed in interacting/merging and starburst galaxies (e.g. Whitmore & Schweizer 1995; Schweizer 1997; Johnson et al. 1999; Goudfrooij et al. 2001; Homeier et al. 2002). (2) Young massive star clusters are observed in "simmering" late-type galaxies. Their number is correlated with the star formation rate per unit area in these systems (Larsen & Richtler 2000). (3) Normalizing the number of globular clusters to the total baryonic mass of the host, reveals a surprisingly constant value (McLaughlin 1999) and points towards a tight link between star and globular cluster formation.

In other words, globular clusters are fossil records of major star-formation episodes in galaxies. Their ages, metallicities, and abundance ratios can provide detailed information on the formation histories of their host systems. As simple stellar populations, globular clusters consist of stars characterized by one age and one metallicity. Hence, the interpretation of their observed colours and spectra is less ambiguous than for the diffuse light. Their ubiquity in all galaxy types and their high surface brightness make them easy to observe out to large distances.

1.2. Spectroscopy of globular cluster systems

Spectroscopy opens an independent way to access ages and metallicities of globular clusters besides photometry. Low resolution spectroscopy ($R \lesssim 1000$) provides information on the strength of prominent diagnostic features, such as the Balmer series and some relatively strong iron and other metal features. Moreover, it can provide clues on the basic chemistry of globular cluster systems.

The Lick index system standardizes the measurement of spectroscopic line indices for many strong absorption features (Burstein et al. 1984; Worthey et al. 1994; Worthey & Ottaviani 1997; Trager et al. 1998). The outstanding role of the Lick system is its provision of index measurements for many stars with a wide range in $\log g$, $T_{\rm eff}$, and [Fe/H]. With this information, so-called fitting functions[1] are computed which are an essential ingredient of theoretical SSP model predictions. Using index response functions[2] (Tripicco & Bell 1995), recent SSP models (Trager et al. 2000a; Thomas et al. 2003, 2004) provide also information on fundamental abundance ratios, such as [α/Fe]. The combination of age-sensitive (e.g. Balmer-line indices) and metallicity-sensitive indices ($\langle$Fe$\rangle$, Mgb, [MgFe]′, etc.) allows in principle to derive accurate spectroscopic ages and metallicities. This approach is less affected by the age-metallicity degeneracy than broadband photometry. In addition, combining indices sensitive to the abundance of α-elements and iron can provide important clues on star-formation time scales (Tinsley 1979; Matteucci 1994; Greggio 1997; Thomas et al. 1999).

The present paper makes use of the spectroscopic data presented in Puzia et al. (2004, hereafter Paper I) to derive global ages, metallicities, and [α/Fe] ratios for globular clusters in early-type galaxies. A more detailed study of these global parameters as a function of internal galaxy properties, such as morphological type, environment, galaxy mass, etc. will be presented in subsequent papers of this series.

We describe the selection of high-quality spectroscopic data in Sect. 2. The best combination of Lick indices to achieve most reliable age and metallicity estimates is discussed in Sect. 3. In Sect. 4 we derive ages and metallicities of globular clusters in the studied early-type galaxies. Global [α/Fe] ratios and correlations with age and metallicity for these globular clusters are presented in Sect. 5. We discuss our results in Sect. 6.

---

[1] A fitting function gives the strength of a specific line index as a function of $\log g$, $T_{\rm eff}$, and [Fe/H].

[2] A response function gives the fractional change of an index as the result of an abundance change of a given element or the total metallicity.

Table 1. Basic information on host galaxies. According to the column the references are: (1) de Vaucouleurs et al. (1991); (2) Tonry et al. (2001); (3) Tully (1988); (4) and (5) Kissler-Patig et al. (1997), Ashman & Zepf (1998).

| Galaxy	Type	$(m - M)_V$	M_B	N_{GC}^a	S_N^b
	(1)	(2)	(3)	(4)	(5)
NGC 1380	−2/LA	31.23 ± 0.18	−20.04	560 ± 30	1.5 ± 0.5
NGC 2434	−5/E0+	31.67 ± 0.29	−19.48	...	...
NGC 3115	−3/L−	29.93 ± 0.09	−19.19	520 ± 120	1.6 ± 0.4
NGC 3379	−5/E1	30.12 ± 0.11	−19.39	300 ± 160	1.2 ± 0.6
NGC 3585	−5/E6	31.51 ± 0.18	−20.93	...	...
NGC 5846	−5/E0	31.98 ± 0.20	−21.16	2200 ± 1300	3.5 ± 2.1
NGC 7192	−4.3/E+	32.89 ± 0.32	−20.55	...	...

[a] Total number of globular clusters.
[b] Specific frequency, $S_N = N_{GC} \times 10^{0.4 \cdot (M_V + 15)}$ (Harris & van den Bergh 1981).

2. Selection of data

Our entire sample contains 143 globular clusters in seven early-type galaxies. About half of our spectra satisfy the ideal S/N standards (~30 per Å) to derive accurate ages, metallicities, and [α/Fe] ratios. It is possible to achieve an age resolution of ~1 Gyr (at ages ~ 15 Gyr) only for the brightest globular clusters in our sample. The typical separation between the 15 and 14 Gyr isochrone in current SSP models is of the order $\Delta H\beta \approx 0.05$ Å, and ~0.1 Å for the higher-order Balmer indices. This separation increases towards younger ages. Hence, the final sample has to be built from a compromise between age/metallicity resolution and sample size. We, therefore, set the selection to clusters with a statistical measurement uncertainty of ≲0.4 Å and ≲0.6 Å for Hβ and higher-order Balmer line indices, respectively. This selection corresponds to a minimum age resolution $\Delta t/t \approx 0.3$. As a metallicity indicator, we use the composite [MgFe]′ index (see below). An error cut at 0.2 Å for this index guarantees a metallicity resolution of ~0.25 dex at high and ~0.4 dex at low metallicities. The above selection criteria leave 71 globular cluster spectra in our sample which correspond to ~50% of the initial data. Henceforth, we consider only these selected globular clusters and combine the data of all sample galaxies to increase statistical significance in the discussed relations. Note, that this sample is biased towards the bright end of the globular cluster luminosity function, i.e. most massive clusters. Otherwise, it spans a wide range in globular cluster color and host galaxy properties (see Table 1).

Our original colour selection criteria prevented us from observing globular clusters with a combination of low metallicities [Z/H] ≲ −1.3 and relatively young ages (t ≲ 5 Gyr). However, these objects are essentially non-existent in our sample galaxies (see Paper I). Figure 1 illustrates the age and metallicity ranges imposed by our colour selection. All Milky Way globular clusters would be selected by our colour cuts 0.8 ≲ $V - I$ ≲ 1.3, 1.5 ≲ $B - I$ ≲ 2.5, and 1.0 ≲ $B - R$ ≲ 1.7 (we refer to Paper I for details). The applied colour cuts also suggest that very metal-rich old globular clusters might be missing in our final sample. We point out that, within our luminosity cut (V ≲ 23 mag), the fraction of such objects amounts only a
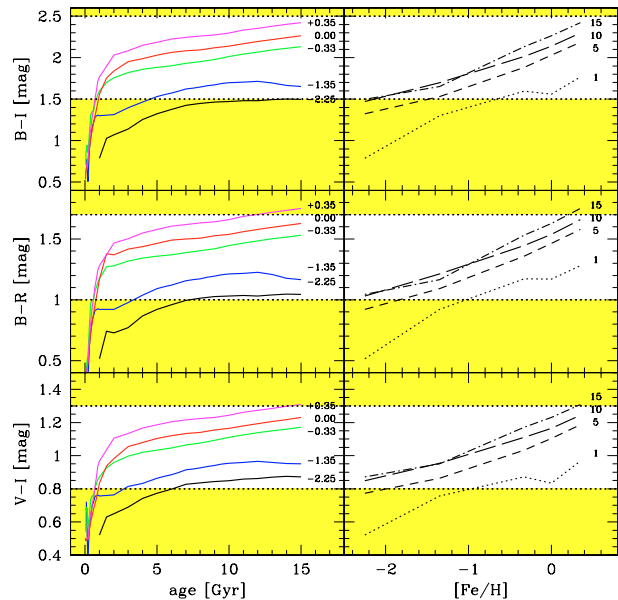
Fig. 1. Illustrated are colours which were used to select globular cluster candidates as a function of age and metallicity and taken from model predictions of Maraston (2005). Upper and lower colour cuts are indicated as horizontal lines. Curves in left panels are parametrized by metallicity, curves in right panels are parametrized by age and indicated accordingly.

few percent. In order to fill the slit-masks we included cluster candidates redder than our colour cuts. However, only two genuine globular clusters were found among ~30 "mask-filler" objects. Unlike the expected old ages, we find intermediate ages (5–10 Gyr) for these two globular clusters. The fraction of old to intermediate-age, very metal-rich globular clusters is likely to increase in a sample reaching fainter magnitudes. However, given our luminosity selection, the number of missed objects is negligible.

Our dataset does not guarantee a strict consistency of the derived mean ages, metallicities and [α/Fe] ratios among the galaxies of our sample. These parameters are subject to change, since neither the sampled fraction of each globular cluster system, nor the sampling of colour distributions and luminosity functions is identical from galaxy to galaxy. Given the still

relatively small numbers of globular clusters per galaxy, a peculiar age and/or metallicity distribution in one galaxy can influence the relation between age, metallicity and [α/Fe] of the complete sample, although we verified that no galaxy represents a clear outlier (see future papers in these series).

## 3. Reducing systematic uncertainties

In the following we determine the best combination of indices as diagnostics for age and metallicity. Taking into account the uncertainty of our line index measurements, the mean uncertainties of the Lick system, and the limits on the predicting power of SSP models, we construct the relatively best combination of diagnostic diagrams from Lick line indices. The found combination maximally reduces the internal uncertainties of the Lick system and the age-metallicity degeneracy of line indices as well as the influence of abundance ratio variations.

3.1. Influence of the blue horizontal branch at high metallicities

As shown by Maraston & Thomas (2000) for Hβ and by Maraston et al. (2003) for the higher-order Balmer lines, the morphology of the Horizontal Branch (HB), when extended to warm temperatures ($\sim$10 000 K), plays a major role in increasing the strength of Balmer indices. This effect is due to metallicity and confuses the use of Balmer lines as pure age indicators (on this topic see also de Freitas Pacheco & Barbuy 1995 and Lee et al. 2000). Since the HB morphology cannot be predicted by first principles of stellar evolution, as it is determined by mass-loss, the line indices need to be calibrated with globular clusters for which the HB morphology is known (Maraston & Thomas 2000; Maraston et al. 2003). This exercise is clearly impossible for extragalactic globular clusters and is the reason why in the following we use both models by Maraston et al. (2003) which include red and blue HB morphologies as a function of metallicity. These models encompass the observed range of Balmer lines in Milky Way globular clusters. As thoroughly explored by Greggio & Renzini (1990), blue HBs are in principle possible also in metal-rich ($Z \gtrsim Z_\odot$) stellar populations (see also Rich et al. 1997, for two examples of metal-rich Milky Way globular clusters with blue HBs), that suffer from enhanced mass-loss and/or have a high helium abundance. Models with blue HBs at high metallicity are published elsewhere (Maraston 2005), and here we report on their differential effect.

To empirically estimate the effect of a varying horizontal branch morphology on Balmer indices at high metallicities, which might be responsible for the increased Balmer indices of metal-rich globular clusters, we parametrize the HB morphology with the HBR parameter (Lee et al. 1994). Figure 2 shows the strength of Balmer line indices as a function of HB morphology (HBR). In general, blue horizontal branches produce significantly stronger Balmer indices for globular clusters in the Milky Way (Trager et al. 1998; Puzia et al. 2002), M 31[3]
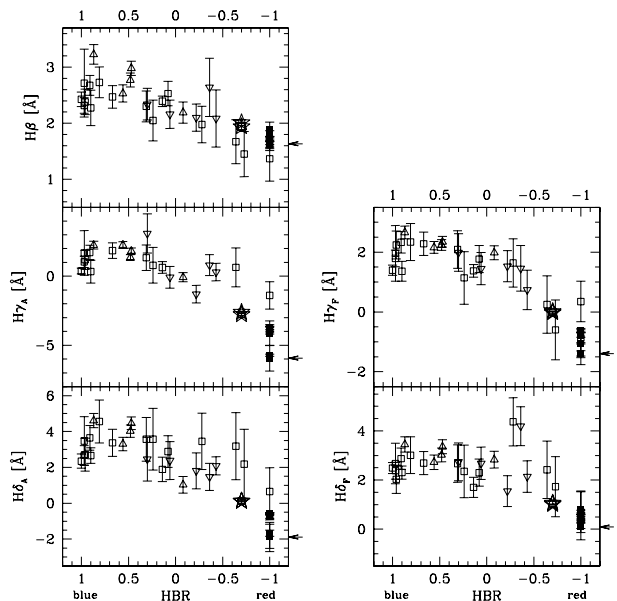
Fig. 2. The behavior of Lick Balmer indices as a function the horizontal branch morphology (HBR). This parameter is defined in Lee et al. (1994) as HBR $(B - R)/(B + V + R)$, where B and R are the number of stars blue-wards and red wards of the instability strip. V is the number of variable stars inside the instability strip. HBR = 1 indicates an entirely blue and HBR = -1 and entirely red horizontal branch. Here we plot data for globular clusters in the Milky Way (*squares*: data from Puzia et al. 2002 and Trager et al. 1998), M 31 (*inverted triangles*: Puzia et al. 2005, Rich et al. 2003, and Trager et al. 1998), and the Large Magellanic Cloud *triangles*: Beasley et al. 2002b). Filled symbols show globular clusters with a metallicity [Z/H] -0.6 (note, all have HBR = -1). NGC 6388 and NGC 6441 are indicated by stars at HBR = -0.7. A small arrow at each panel's right ordinate indicates the most extreme Balmer index value for globular clusters with [Z/H] > -0.6. Several clusters show a tendency for higher Balmer indices at HBR ≈ -0.5. Their deviations from the overall sequence are $\leq 2\sigma$.

(Trager et al. 1998; Puzia et al. 2005), and the LMC (Beasley et al. 2002b). Each panel shows a sequence of metallicity, where the scatter can be attributed to the "second parameter". We use the globular clusters NGC 6388 and NGC 6441 (which host the bluest horizontal branches among metal-rich Galactic globular clusters, indicated by stars in Fig. 2) and clusters at [Z/H] $\gtrsim -0.6$ (filled symbols) which have entirely red HBs (e.g. NGC 6356 and NGC 6637) to derive a representative "second-parameter" variation of Balmer line indices at high metallicities. As this approach is fully empirical and based on the largest HB morphology fluctuation locally observed, we cannot rule out that even more extreme HB morphologies for globular clusters at a given metallicity exist outside the Local Group. We find, in the extreme case, offsets of 0.4 Å in Hβ, 3.3 Å in Hγ_A, 1.4 Å in Hγ_F, 2.0 Å in Hδ_A, and 1.0 Å in Hδ_F between metal-rich globular cluster with the *weakest* Balmer index (with entirely red HBs) and NGC 6388 and 6441. The HB morphology has negligible effect on the [MgFe]$'$ index. Consequently, increased Balmer indices at high metallicities might well be, at least partly, the result of HB morphology variations.

In the following we use the Balmer indices as age indicators with confidence at low metallicity ([Z/H] $\lesssim -0.6$), because
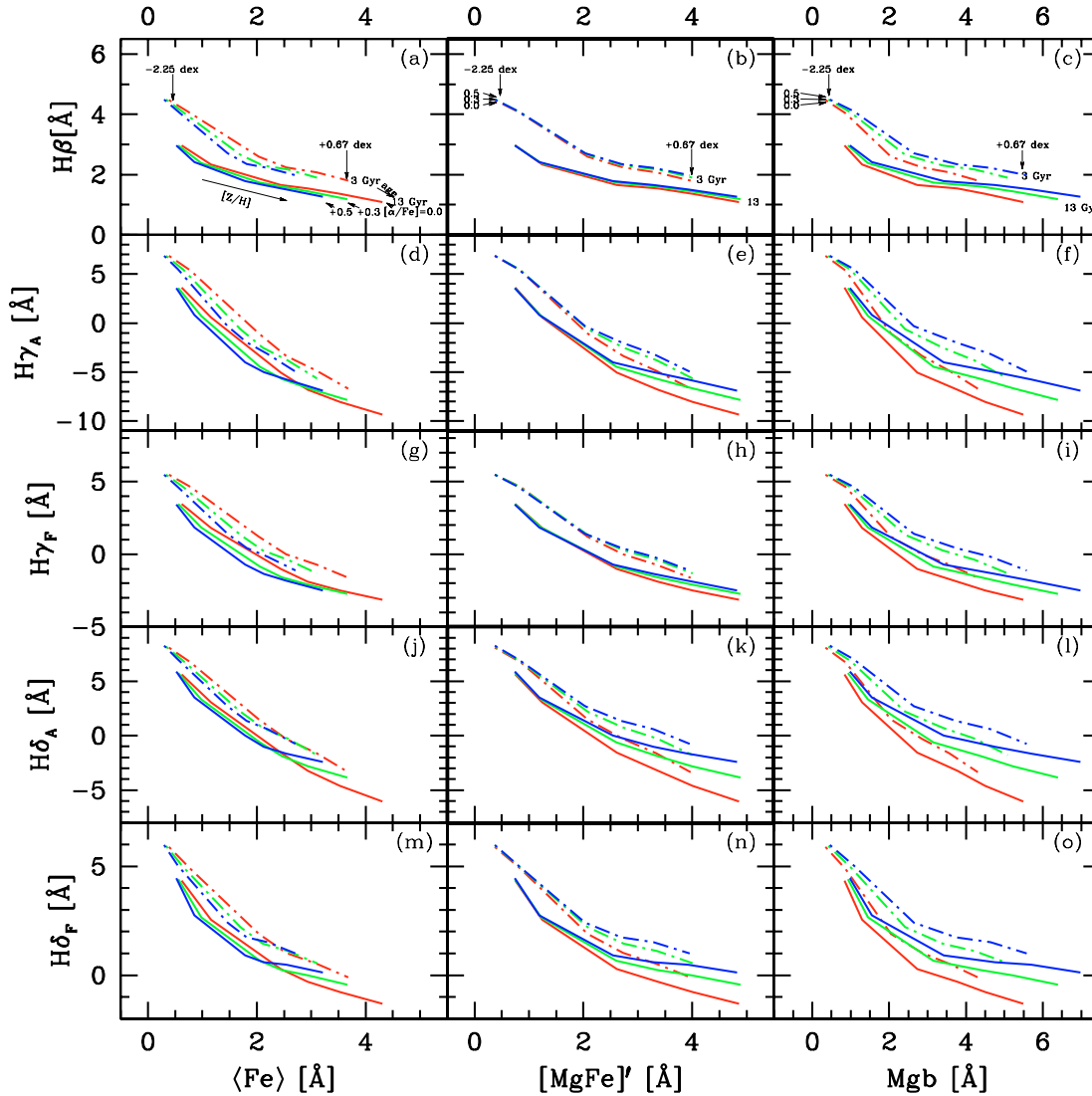
Fig. 3. Influence of [α/Fe] variations on age-metallicity diagnostic grids. Panel **a)**: Hβ vs. ⟨Fe⟩. Lines show model predictions (Thomas et al. 2003, 2004) for stellar populations with metallicities [Z/H] = −2.25 to 0.67 dex and two ages 13 (solid lines) and 3 Gyr (dot-dashed lines) parametrized for three different [α/Fe] ratios 0.0, 0.3, and 0.5 dex. Panel **b)** shows the same model predictions for Hβ vs. [MgFe]′, while panel **c)** illustrates the changes in the Hβ vs. Mgb grid. The other panels show the predicted variations for higher-order Balmer line age/metallicity diagnostic grids.

HB morphology is included in our SSP models and under control. At high metallicity ([Z/H] ≳ −0.6), we have the warning in mind that ages could be degenerate with the presence of unresolved blue HBs. For this reason we will refer to such young ages as "formal".

3.2. The influence of [α/Fe] variations on iso-age tracks

Recently, Thomas et al. (2003, 2004) calculated new theoretical Lick index predictions which are parametrized for *well-defined* [α/Fe] ratios for a wide range of ages and metallicities. These models take into account the effects of changing element abundance ratios on Lick indices, hence give Lick indices not only as a function of age and metallicity, but also as a function of the [α/Fe] ratio. They are based on the evolutionary

population synthesis code of Maraston (1998). The impact from element-ratio changes is computed with the help of the Tripicco & Bell (1995) and Korn et al. (2005) response functions, using an extension of the method introduced by Trager et al. (2000a). Because of the inclusion of element-ratio effects, the influence of [α/Fe] on Balmer indices can be studied, and is illustrated in Fig. 3. Here we show the influence of [α/Fe] variations on frequently used age/metallicity diagnostic diagrams. In general, variations of Balmer-line indices for isochrones with [α/Fe] ratios between solar and +0.5 dex are of the order ~0.007−0.25 Å for low, and ~0.18−3.63 Å for high metallicities, and introduce a relative age uncertainty in the range Δt/t ~ 0.1−0.2. These variations are due to different contaminations by metal absorption features inside the Balmer index passband definitions, as illustrated in Fig. 4. The figure shows the higher-order Balmer indices generally include more metal absorption lines in their feature and pseudo-continuum
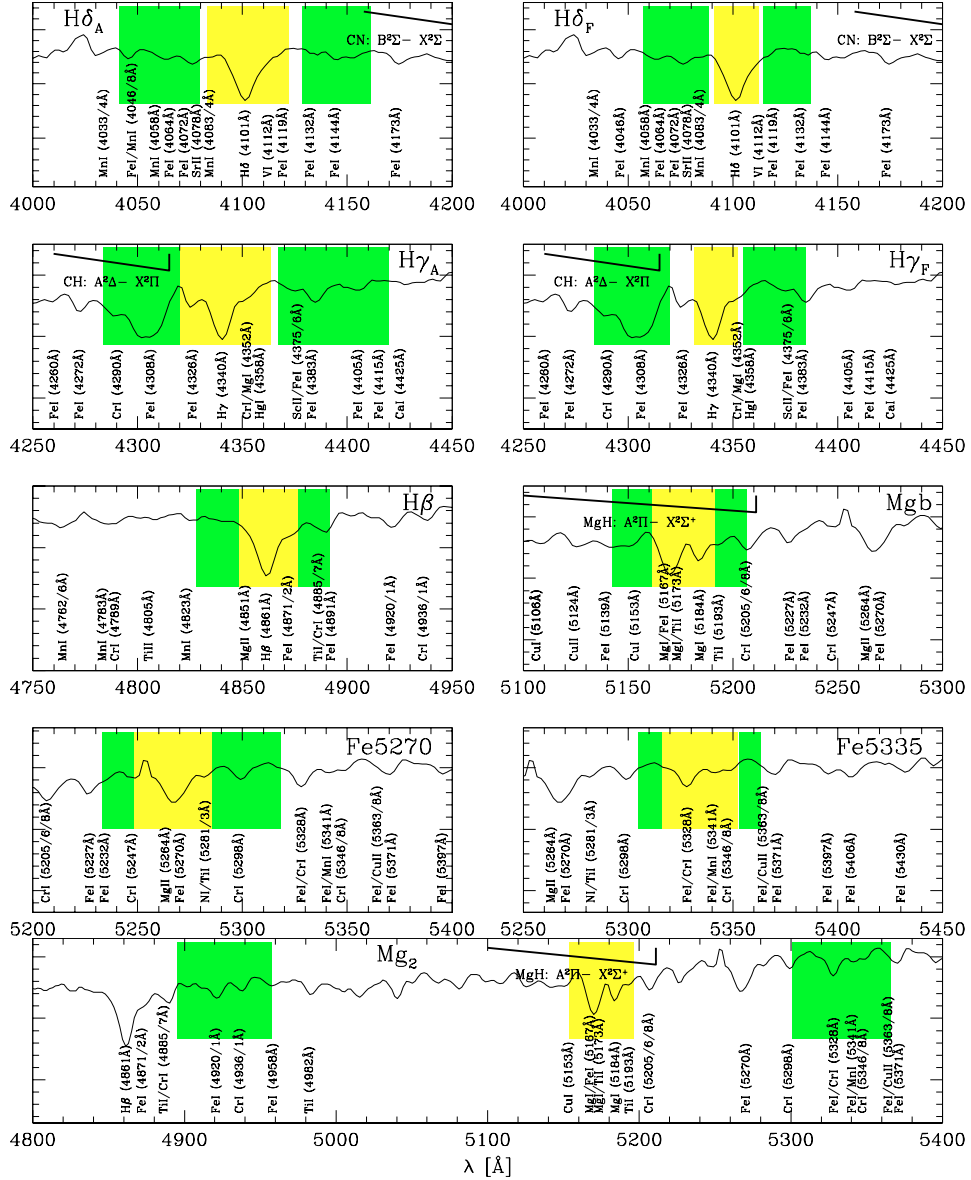
Fig. 4. Passband definitions for Balmer-line, Mgb, Fe5270, and Fe5335 Lick indices with their feature and adjacent continuum passbands. The over-plotted spectrum is a high-S/N spectrum of the Galactic globular cluster NGC 6284 (Puzia et al. 2002). The resolution is ~7 Å and was left untouched to keep satellite lines visible. Line data were taken from Reader & Corliss (1981), data for molecular bands are from Rosen (1952). Note the large number of satellite lines which are included in the passband definitions.

passbands than the Hβ index, which is the Balmer index with the narrowest passband definitions. Hence, among all Lick Balmer line indices, the least [α/Fe]-sensitive index is Hβ, followed by Hγ_F, Hγ_A, Hδ_A, Hδ_F (see also Thomas et al. 2003, 2004). This exercise demonstrates that at high metallicities the impact of [α/Fe] variations on age/metallicity determinations (in particular, those of early-type galaxies) can significantly alter the results and/or introduce spurious correlations.

3.3. The relatively best age indicator

The Balmer line series provides the best spectroscopic age indicator among the set of Lick line indices. The Lick system defines five indices (Hβ, Hγ_A, Hδ_A, Hγ_F, and Hδ_F) for three Balmer lines (Worthey et al. 1994; Worthey & Ottaviani 1997).

Figure 4 shows the passband definitions for all Balmer indices. In combination with a metallicity diagnostic, these higher-order Balmer line indices are widely used to determine (luminosity-weighted) ages and metallicities of galaxies (e.g. Trager et al. 1998, 2000a,b; Kuntschner 2000; Poggianti et al. 2001; Kuntschner et al. 2002a; Thomas et al. 2003).

However, different types of diagnostic plots based on different Balmer-line indices are used throughout the literature. Although the age predicting power of an arbitrarily chosen diagnostic plot (most common versions include the Hβ and Mg$_2$ or $\langle$Fe$\rangle$ indices might yield accurate-enough results for a specific scientific goal (e.g. the mean age difference between two different galaxy samples), the choice of a specific diagnostic plot is still subject to observational constraints and individual assessment, and makes comparisons between studies

Table 2. Summary of the coefficients relevant to Eq. (1). The coefficients in Cols. 2–8 are given in units of Å. Columns 9–14 are given in dex/Gyr. Note that for the higher-order Balmer indices Col. 5 gives the arithmetic mean of the uncertainties for cool and warm stars (see Tables 3 and 4 in Worthey & Ottaviani 1997).

index	η	ζ	γ	δ	$\mathcal{D}_{-1.35}$	$\mathcal{D}_{0.0}$	$\langle\mathcal{D}_Z\rangle$	$\mathcal{S}_{0.3,-1.35,3}$	$\mathcal{S}_{0.3,-1.35,13}$	$\mathcal{S}_{0.3,0,0,3}$	$\mathcal{S}_{0.3,0,0,13}$	$\langle\mathcal{S}_{\alpha,Z,t}\rangle$	$\mathcal{R}$
1	2	3	4	5	6	7	8	9	10	11	12	13	14
Hβ	0.20	0.232	0.22	1.30	2.55	2.68	2.62	0.382	0.137	0.408	0.102	0.257	0.497
Hγ_A	0.28	0.722	0.48	1.78	7.75	11.01	9.38	0.283	0.068	0.227	0.036	0.154	0.722
Hγ_F	0.28	0.448	0.33	1.34	4.55	5.83	5.19	0.291	0.072	0.123	0.050	0.134	0.471
Hδ_A	0.27	1.043	0.64	1.27	5.73	9.11	7.42	0.259	0.045	0.180	0.032	0.129	0.537
Hδ_F	0.28	0.790	0.40	1.18	3.83	4.47	4.15	0.281	0.052	0.114	0.036	0.121	0.334

difficult. As a consequence, most authors use several diagnostic plots with different Balmer line indices and assign equal importance to the results derived from each of those.

In the following we provide a recipe to define a quantity from which the relatively best Balmer-line age indicator can be determined. This quantity takes into account the quality of a given dataset and the diagnostic power of theoretical predictions from which one intends to derive the age and metallicity. It does not take into account *systematic* uncertainties in the fitting functions for a particular index.

In particular, the age sensitivity of an index is a function of the following parameters:

- η: mean error of the data in Å;
- ζ: transformation accuracy to the Lick system in Å;
- γ: mean error of the original Lick spectra in Å;
- δ: accuracy of the Lick fitting functions in Å (Worthey et al. 1994; Worthey & Ottaviani 1997);
- $\mathcal{D}_Z$: index range in Å covering all ages at a given metallicity, hereafter termed the dynamic range;
- $\mathcal{S}_{\alpha,Z,t}$: degeneracy parameter, which quantifies the sensitivity of an index I to age, metallicity, and α/Fe ratio at a given $[\alpha/\text{Fe}]$, metallicity, and age (i.e. the impact of the age-metallicity and age-α/Fe degeneracy), given in dex/Gyr.

The numerical values for each parameter are given in Table 2 for each Balmer index. It is worth noting that some of these values are only valid for our data quality in combination with the SSP models of Thomas et al. (2003, 2004). For different data and SSP models, η, $\mathcal{D}_Z$, and $\mathcal{S}_{\alpha,Z,t}$ are subject to change. To quantify the most age-sensitive and least metallicity-sensitive Balmer index, we define the quantity

$$\mathcal{R} = \frac{\mathcal{D}_Z \cdot \mathcal{S}_{\alpha,Z,t}}{\sqrt{\eta^2 + \zeta^2 + \gamma^2 + \delta^2}} \tag{1}$$

where the degeneracy parameter, $\mathcal{S}_{\alpha,Z,t}$, is defined as

$$\mathcal{S}_{\alpha,Z,t}(I) = \left|\frac{\partial I}{\partial t}\right|_{Z,\alpha} \cdot \left(\left|\frac{\partial I}{\partial[Z/H]}\right|_{\alpha,t}^2 + \left|\frac{\partial I}{\partial[\alpha/\text{Fe}]}\right|_{Z,t}^2\right)^{-\frac{1}{2}} \tag{2}$$

$\mathcal{R}$, which is given in dex Gyr^{-1}, is essentially the dynamic range of an index I at a given age and metallicity expressed in units of the total uncertainty. We use the mean dynamic age range $\mathcal{D}_Z$ at two different metallicities $[Z/H] = -1.35$ and 0.0 between the 1 and 15 Gyr isochrone. Each SSP model provides a well-defined relative age scale which we use here to

parametrize $\mathcal{S}_{\alpha,Z,t}$ for two different metallicities $[Z/H] = -1.35$ and 0.0, two different ages 3 and 13 Gyr, and $[\alpha/\text{Fe}] = 0.3$. $\mathcal{S}_{\alpha,Z,t}$ is the ratio of age, metallicity, and $[\alpha/\text{Fe}]$ partial derivatives (see Eq. (2)). In other words, $\mathcal{S}_{\alpha,Z,t}$ is a measure of the age-metallicity and age-α/Fe degeneracy, and is maximal for indices which are most sensitive to age and least sensitive to metallicity and $[\alpha/\text{Fe}]$ variations, at the same time.

The highest $\mathcal{R}$ indicates the best age indicator with least age-metallicity and age-α/Fe degeneracy. In Table 2 we provide values for $\mathcal{D}_Z$ at two different metallicities and for $\mathcal{S}_{\alpha,Z,t}$ at $[\alpha/\text{Fe}] = 0.3$ and four age-metallicity combinations for each Balmer line index. Since SSP models do not provide continuous but discrete predictions the partial derivatives are substituted by difference ratios, e.g. $\partial I/\partial t \rightarrow \Delta I/\Delta t$. The quotients are determined by linear interpolation of SSP models.

We determine the relatively best age indicator from the set of five Lick Balmer indices by combining the mean dynamic range $\langle\mathcal{D}_Z\rangle$, the mean age-metallicity and age-α/Fe degeneracy parameter $\langle\mathcal{S}_{\alpha,Z,t}\rangle$, and the total index uncertainty which is the denominator in Eq. (1). The final mean $\mathcal{R}$ is documented in the last column of Table 2. We find that the relatively best age diagnostic for our data is the Hγ_A index followed by the indices Hβ and Hδ_A. Hγ_F and Hδ_F have the smallest $\mathcal{R}$ values and are not considered to be reliable age indicators.

It is instructive to see that despite the relatively large age-metallicity degeneracy of the Hγ_A index, it still provides the most accurate age predictions. This fact is primarily due to the large dynamic range of Hγ_A compared to its mean measurement uncertainty. Hβ, on the other hand, has a relatively large total uncertainty and the measurements will therefore be more scattered over the diagnostic plot's parameter range. However, Hβ shows by far the highest $\langle\mathcal{S}_{\alpha,Z,t}\rangle$ value (Col. 13 in Table 2; see also Fig. 3) and is therefore least sensitive to the cumulative effects of age-metallicity and age-α/Fe degeneracy. In general, the higher-order Balmer lines require less S/N to guarantee a similar total index accuracy as Hβ, which is primarily due to the narrow passband definition of Hβ (see Fig. 4). If our dataset would be infinitely accurate (i.e. $\eta = 0$ in Eq. (1)), the order of $\mathcal{R}$ from the best to worst Balmer index would remain unchanged. The value of $\mathcal{R}$ is predominantly governed by uncertainties in the fitting functions of the respective index. To vary this order, the mean measurement uncertainties have to be very discrepant and the SSP-model predictions have to deviate significantly from the model used here. It is expected that the

relative accuracy of Balmer index measurements is comparable between different datasets as they are usually derived from one optical spectrum. The *relative* age scale of SSP models appears to be quite stable against the choice of different stellar evolutionary tracks for ages > 1 Gyr (Charlot et al. 1996; Trager et al. 2000a; Maraston 2003). This scale is used in our above prescription. It can therefore be expected that no large fluctuation in $\mathcal{R}$ will arise from the use of different SSP model predictions[4].

3.4. The relatively best metallicity indicator

The index with the highest metallicity sensitivity and minimal age-sensitivity could in principle be found in a comparable way as it was done for the relatively best age diagnostic. The major impact of typical metallicity tracers, such as $\langle\text{Fe}\rangle$, Mg_2, and $\text{Mg}b$, on the absolute metallicity scale is expected to arise from changing abundance ratios. To reduce the influence of $[\alpha/\text{Fe}]$ variations on age and metallicity determinations, Thomas et al. (2003) modify the [MgFe] index[5] to obtain an $[\alpha/\text{Fe}]$-*insensitive* metallicity index,

$$[\text{MgFe}]' = \sqrt{\text{Mg}b \cdot (0.72 \times \text{Fe}5270 + 0.28 \times \text{Fe}5335)}.$$

Figure 3 shows the behavior of isochrones in three different frequently used diagnostic plots. The middle column impressively illustrates that [MgFe]', indeed, is essentially independent of $[\alpha/\text{Fe}]$. Henceforth, we adopt the [MgFe]' index as the best metallicity indicator and use it in combination with selected age indicators (see Sect. 4.1) to derive ages, metallicities, and $[\alpha/\text{Fe}]$ ratios for our sample globular clusters.

3.5. Excluding contamination by ionized gas

It is known that ∼40−60% of early-type galaxies show indications of emission in their absorption spectra (Caldwell 1984; Phillips et al. 1986; González 1993; Goudfrooij et al. 1994). In a narrow-band imaging survey, Macchetto et al. (1996) find ionized gas in ∼80% of early-type galaxies including flocculent Hα+[NII] emission in NGC 3379, NGC 5846, and NGC 7192, well within ∼1 R_{eff}, but no significant emission in NGC 3115. This gas is located in the central parts and distributed in a rather regular way, suggestive of a disk. If dominant, all Balmer indices would be affected, along with potential contamination of Fe5015 by [OIII] (λ 5007 Å) and of Mgb by [NI] (λ 5199 Å) (Goudfrooij & Emsellem 1996). In that case, our measurements would indicate *too old ages*. This effect rapidly decreases from Hβ towards Hγ and Hδ (Osterbrook 1989), i.e. higher-order Balmer indices are less affected and should be preferentially used for age determinations in the presence of ionized gas.

In order to exclude a major effect of ionized gas on line-strength measurements in our globular cluster data, we performed several tests/estimates.

Since line emission is concentrated in the central parts of galaxies (Macchetto et al. 1996), we expect a correlation of Balmer indices with galacto-centric radius if line-emission contamination is significant. We find no evidence that Balmer indices are correlated with galacto-centric distance. A more detailed analysis of background spectra shows that most clusters are located within ∼2−3 R_{eff} and that the flux level of the diffuse galaxy light is well below the object flux. In particular, we find no correlation inside one effective radius, where line emission is expected to be strongest. Furthermore, we find no correlations of Balmer indices for globular clusters with Balmer indices measured on corresponding background spectra.

Visual re-inspection of the background subtraction process for some low-Hβ outliers (see Fig. 6) underline the good quality of background modeling and subtraction. However, problems with accurate background subtraction might occur in very few cases when line emission has a very filamentary structure. For instance, the worst case scenario would be when a globular cluster overlaps with a filament of ionized gas while the slit is aligned perpendicular to such a filament. However, a filamentary emission pattern is not found in the Macchetto et al. (1996) study for our host galaxies. We conclude that line emission has no measurable effect on the scatter in the age/metallicity and $[\alpha/\text{Fe}]$ diagnostic plots.

4. Ages and metallicities

4.1. Iterative method

Having determined the relatively best metallicity diagnostic, we determine the best combination of Balmer-line indices as our prime age indicator. In deciding whether a Balmer index will be chosen as part of this most reliable age proxy, we inspect the following points for each Balmer index and assign priorities in descending order:

a) ranking of the reliability parameter $\mathcal{R}$, as described in Sect. 3.3;
b) including the maximum number of the Balmer lines without duplicate measurements by two or more line indices.

We choose the combination of $\text{H}\gamma_A$, Hβ, and $\text{H}\delta_A$ as our most reliable age indicator. Consequently, ages and metallicities for individual globular clusters are computed as the weighted mean of the parameters derived from diagnostic plots constructed from these three Balmer indices vs. [MgFe]'. As weights we choose the reliability parameters $\mathcal{R}$ from Table 2.

Since the SSP model predictions allow full control over $[\alpha/\text{Fe}]$ variations within the diagnostic grids, we use an iterative approach in combination with a second diagnostic grid from which we derive the $[\alpha/\text{Fe}]$ ratios (Mg_2 vs. $\langle\text{Fe}\rangle$, see Sect. 5). As a first step the α-enhancement for each individual globular cluster is derived. This value is used to interpolate the age/metallicity diagnostic grid for the correct α-element enhancement. From so adjusted grids ages and metallicities are computed using linear interpolation of the model predictions employing a least-square technique. These ages and metallicities are then used to adjust the $[\alpha/\text{Fe}]$ diagnostic grid, which

---

[4] We note that systematic uncertainties in the fitting functions and effects of emission-line filling are not considered by this exercise.

[5] $[\text{MgFe}] = \sqrt{\text{Mg}b \cdot \langle\text{Fe}\rangle}$, see González (1993).
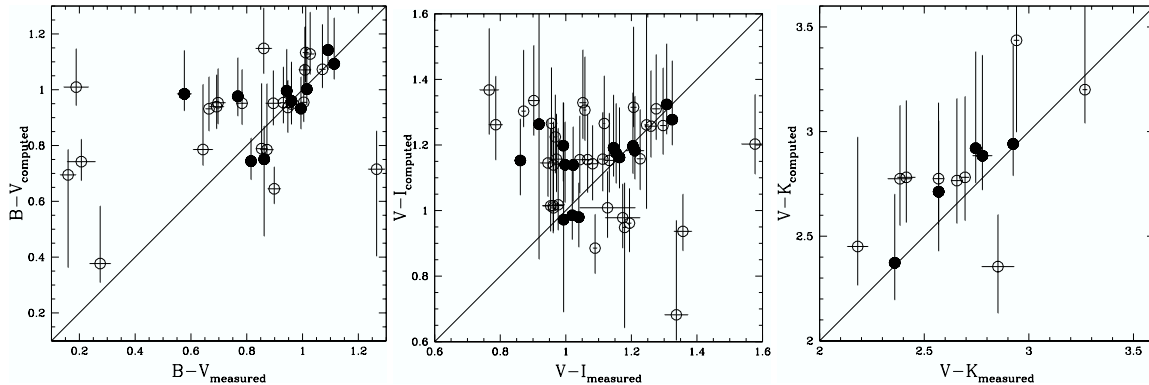
Fig. 5. Computed vs. measured photometric colors for our sample globular clusters. Computed colors were derived from spectroscopic ages and metallicities using the SSP models of Maraston (2005). The circles show all selected globular clusters for which optical/near-infrared colors were obtained (see Paper I for details). Solid circles show the high-quality sample, which was selected by a more constrained error cut (see text for details). Errorbars indicate 1-σ uncertainties.

itself is slightly dependent on age. This procedure is iterated until the age, metallicity, and [α/Fe] values converge. Extensive tests show that this goal is reached within a few iteration steps. Along with these values we also determine the statistical errors due to index measurement uncertainties. Typically the errors are asymmetric which is a result of the skewness of diagnostic grids (see Fig. 6).

For objects which fall outside the diagnostic grid, we assign the most likely extreme grid value and do *not* extrapolate the model predictions, i.e. we project the data onto the closest grid point along its error vector[6]. Note that due to the increasing influence of hot blue horizontal-branch stars, the iso-age tracks for old ($t > 8$ Gyr) stellar populations with metallicities below -1.0 dex tend to overlap. This introduces an ambiguity in assigning ages and metallicities to individual globular clusters and artificially broadens the age distributions at old ages. However, only six objects are affected by this ambiguity which has no effect on the following results. For these six objects the routine randomly assigns either young or old ages and the corresponding metallicities.

4.2. Consistency checks

The comparison of derived formal ages and metallicities of individual globular clusters shows that different diagnostic diagrams make *age* predictions which are somewhat inconsistent with one another. The average relative age uncertainty varies in the range $\Delta t/t \approx 0.2$–0.5 which we attribute to systematic errors in the age scale of model predictions and/or systematics in the calibration of the data. By combining age predictions from different diagnostic plots we smooth out these systematic effects which influence age determinations derived from single Balmer indices.

This age inconsistency is partly surprising as the Maraston et al. (2003) models are well calibrated for Milky Way globular clusters and their ages derived from different Balmer indices are consistent with each other.
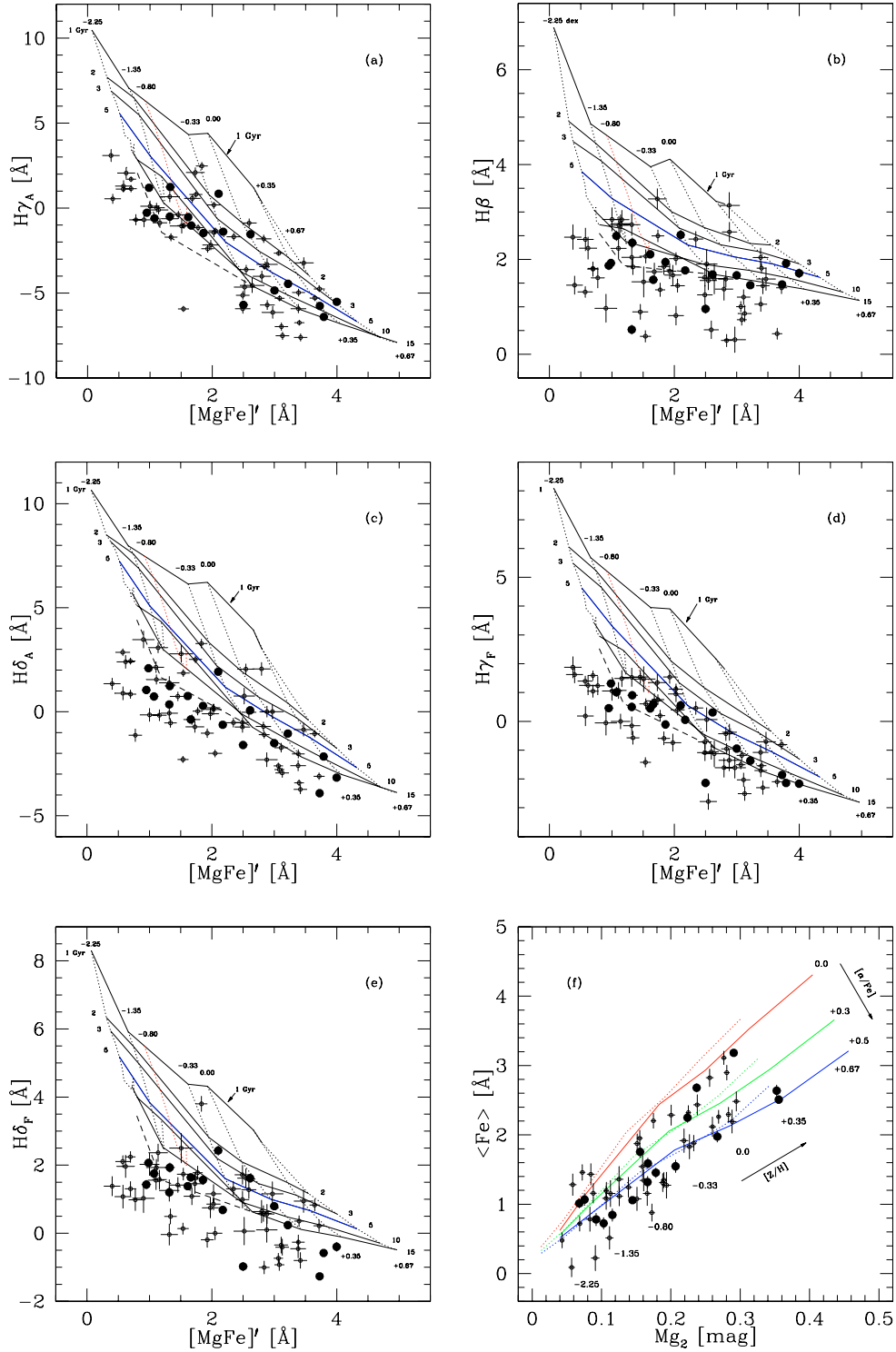
On the other hand, we find very good agreement of metallicity predictions from all diagnostic plots within an average uncertainty of ~0.2 dex.

Note also, that a striking feature of all age/metallicity diagnostic plots in Fig. 6 is that a significant fraction of globular clusters lie below the oldest iso-age track. This is observed in other samples of *extragalactic* globular clusters in the literature as well (e.g. Kissler-Patig et al. 1998; Cohen et al. 1998; Puzia et al. 2000; Larsen et al. 2003). Systematics in the data reduction have been deemed extremely unlikely given the good Lick standard calibration (see Paper I) and are also unlikely given the general problem in the literature. We could also exclude emission filling as source for the Balmer index inconsistencies which is presented in Sect. 3.5.

To test whether the spectroscopic age and metallicity predictions for these outliers are consistent with their observed photometric colors (see Paper I for details), we use SSP models of Maraston (2005) to compute photometric colors from the derived spectroscopic ages and metallicities. Figure 5 shows the comparison of computed and observed data. We find good agreement for the $B - V$, $V - I$, and $V - K$ colors. We find no systematics in color residuals as a function of Balmer index with respect to the one-to-one relation. However, we find significantly smaller residuals towards more metal-rich objects.

We also investigate if higher-quality data alleviates these inconsistencies and select a sub-sample with statistical errors $\Delta H\beta < 0.11$ Å and $\Delta H_{\gamma,\delta} < 0.165$ Å for higher-order Balmer lines, which is shown as solid dots in Fig. 5. For this sub-sample, we indeed find a better agreement between computed and observed photometric colors. We take this as an indication that the age and metallicity predictions for the higher-quality dataset are more robust. Based on our photometric cross-check, we only consider the ages and metallicities derived for our high-quality sub-sample as trustworthy. However, to illustrate the difference between the high-quality and the rest of the data we plot the remaining dataset in the following diagnostic plots as open symbols in Fig. 6 and show their distributions as hatched histograms in Fig. 7.

---

[6] To illustrate the effect of this procedure we mark objects, which fall off the grid in all diagnostic plots, by double-hatched histogram in the distributions plots in Fig. 7.

Fig. 6. Age-metallicity diagnostic plots (panels **a)**–**e)**) constructed from Balmer indices Hγ_A, Hβ, Hδ_A, Hγ_F, and Hδ_F vs. [MgFe]′ for high-quality globular cluster spectra (solid dots). Open circles show our remaining selected globular cluster data. SSP models of Thomas et al. (2004) have been over-plotted for [α/Fe] = 0.3, metallicities [Z/H] = $-2.25, -1.35, -0.80, -0.33, 0.00, 0.35,$ and 0.67 dex (dotted lines), and ages 15, 10, 5, 3, 2, 1 (solid lines). The red dotted line is an interpolated iso-metallicity track for [Z/H] = -0.8. The blue solid line is the 5 Gyr isochrone, and is used to split between old and young globular clusters. A *dashed isochrone* illustrates the Balmer index strengths for a 15 Gyr old stellar population with an entirely red horizontal-branch morphology. The [α/Fe] diagnostic plot (panel **f)**) shows the mean iron index ⟨Fe⟩ as a function of Mg$_2$. SSP models of Thomas et al. (2003, 2004) with constant [α/Fe] ratios have been over-plotted for [Z/H] between -2.25 and $+0.67$ dex and two ages 13 (*solid lines*) and 3 Gyr (*dotted lines*) with various [α/Fe] ratios 0.0, +0.3, and +0.5 dex.

4.3. Results

In the following, we discuss ages and metallicities for the high-quality sub-sample derived from diagnostic plots using the Balmer-line indices Hβ, Hγ_A, and Hδ_A (see Sect. 4.2). The corresponding diagnostic diagrams are shown in Fig. 6 along with the other two diagrams constructed from the Balmer indices Hγ_F, and Hδ_F. Since for seven globular clusters one or more of the three Balmer indices Hβ, Hγ_A, and Hδ_A are not available, we exclude these objects from the subsequent analysis to avoid systematics, which leaves 17 globular clusters in our high-quality sub-sample. Their age and metallicity distributions are shown in Fig. 7 as solid histograms.

Our method reveals that a significant fraction of clusters in the high-quality sample (6/17 or 35%, see solid histogram in Fig. 7) has formal ages between 5 and 10 Gyr. Only one object has a formal age below 5 Gyr (~3.8 Gyr) and there are no globular clusters with extremely young ages ($\lesssim$1 Gyr). We split the sample at [Z/H] = −0.6, corresponding to the dip in the Milky Way globular cluster metallicity distribution (Harris 1996), into metal-poor and metal-rich globular clusters. With this distinction we find an increase in age spread from metal-poor to metal-rich clusters. We derive a dispersion of 0.5 Gyr for metal-poor and a dispersion of 3.5 Gyr for metal-rich globular clusters. A weighted linear least-square fit to our high-quality dataset reveals a weak age-metallicity relation, in the sense that more metal-rich globular clusters appear on average younger. The significance of this relation needs to be tested with larger samples.

Our high-quality globular cluster sample covers metallicities in the range −1.3 $\lesssim$ [Z/H] $\lesssim$ +0.5, with a mean −0.36 ± 0.13 and dispersion σ = 0.52 dex. Four out of 17 globular clusters have formally super-solar metallicities. All clusters that are younger than 10 Gyr have metallicities [Z/H] $\gtrsim$ −0.4, which excludes their formation from primordial gas clouds.

We note that no super metal-rich, intermediate-age counterpart globular cluster population is found in the Milky Way (e.g. Harris 2001). However, globular clusters with intermediate ages are found in M 31 (e.g. Barmby et al. 2000; Burstein et al. 2004; Beasley et al. 2004; Puzia et al. 2005), whose bulge-to-disk ratio is larger than that of the Milky Way. An interesting idea is that this mode of globular cluster formation may not have manifested itself in our Galaxy due to Milky Way's smaller bulge (Goudfrooij et al. 2003).

In summary, the conclusions that can be drawn from our previous analysis of globular clusters in early-type galaxies are the following:

- metal-poor globular clusters are on average older than metal-rich globular clusters;
- there is a tendency for metal-rich globular clusters to have a younger mean age relative to their metal-poor counterparts;
- metal-rich globular clusters exhibit on average a larger age spread than metal-poor globular clusters.

5. [α/Fe] ratios

In this Section we derive [α/Fe] ratios for our high-quality sample globular clusters using a diagnostic diagram which is
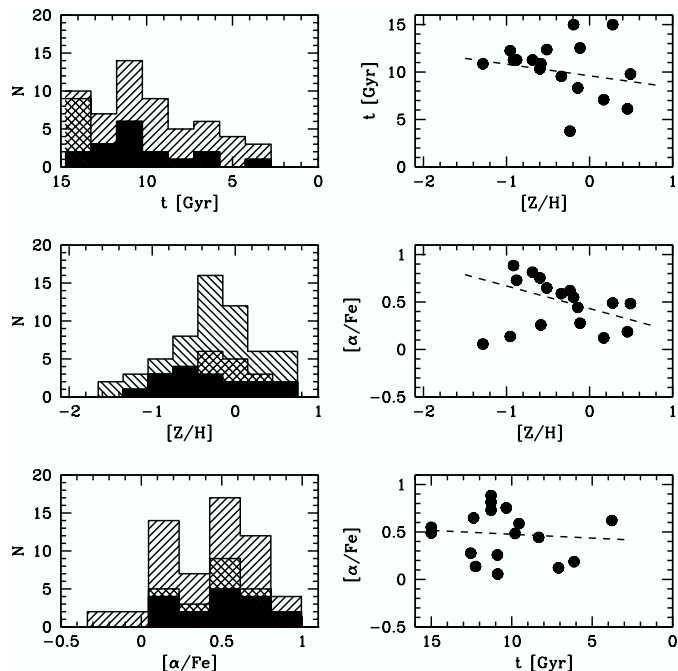
Fig. 7. Histograms for ages, metallicities, and [α/Fe] ratios for globular clusters in early-type galaxies. The panels in the left column show distribution of each parameter for all selected (hatched histograms), outliers in diagnostic plots (double-hatched histograms), and high-quality data (solid histograms). Each panel in the right column illustrates a correlation of two of these parameters for the high-quality sub-sample. Dashed lines in the correlation plots show weighted least-square fits.

least sensitive to age/metallicity variations. Such a diagram can be constructed from the indices $\langle$Fe$\rangle$ and Mg$_2$, which primarily trace the abundances of iron and the α-element magnesium (Tripicco & Bell 1995). We note that among the three Mg-sensitive indices, Mg$_1$, Mg$_2$, and Mgb, theoretical index predictions show a relatively large spread in $\langle$Fe$\rangle$ and Mg$_2$ for [α/Fe] ratios between solar and ~0.5 dex, at high mean metallicities. Given the quality of our data we can expect a good discrimination between enhanced and solar-type [α/Fe] ratio for individual globular clusters at metallicities [Z/H] $\gtrsim$ −0.8 and a good estimate of the mean [α/Fe] ratio at lower metallicities.

Figure 6 (panel f) shows that the Mg$_2$ vs. $\langle$Fe$\rangle$ diagnostic diagram is not entirely free from the age/metallicity degeneracy. Iso-[α/Fe] tracks for three different ratios (0.0, 0.3, and 0.5 dex) are plotted for two ages (3 and 13 Gyr, indicated by dotted and solid lines, respectively). It is obvious that age information is needed to choose the correct set of tracks for a reliable [α/Fe] determination. The diagnostic grid is interpolated in our iterative fitting routine using information derived from age/metallicity diagnostic grids (see Sect. 4.1). In other words, [α/Fe] ratios are determined simultaneously with ages and metallicities. The averaging is identical to the one for ages and metallicities in Sect. 4.1.

A histogram of [α/Fe] ratios for our high-quality sample is shown in Fig. 7. *All* globular clusters are consistent with

super-solar [α/Fe] ratios. The mean [α/Fe] of the sample is 0.47 ± 0.06 dex, with a dispersion of 0.26 dex.

Using a weighted linear least-square fit, we find evidence for a [α/Fe]–metallicity relation in the sense that more metal-rich globular clusters have lower [α/Fe] ratios. However, due to the reduced [α/Fe] resolution of Lick indices at low metallicities and our modest sample size (especially at the metal-poor end), this trend needs to be confirmed with more data. Consistent with the previously found age–metallicity and [α/Fe]–metallicity relation, we find no evidence for a [α/Fe]–age correlation. Globular clusters at all ages appear to have on average super-solar [α/Fe] ratios.

Recent measurements of [α/Fe] ratios in globular cluster systems in other early-type galaxies reveal very similar results. For instance, the data of Kuntschner et al. (2002b) for globular clusters in NGC 3115 show that most clusters are consistent with [α/Fe] $\approx$ 0.3 over the entire range of sampled metallicities. Larsen et al. (2002b) find a super-solar mean [α/Fe] ratio of +0.4 dex for globular clusters of all metallicities in NGC 4594 (Sombrero). Using SSP models with non-constant [α/Fe] ratios, Forbes et al. (2001) argue that at least some globular clusters in NGC 1399 exhibit super-solar [α/Fe] ratios. However, the found [α/Fe]–metallicity correlation is seen in this sample for the first time. This is mainly due to the higher quality of our data and a more reliable age/metallicity determination compared to previous studies.

Note that super-solar [α/Fe] ratios have also been reported for the *diffuse light* of early-type galaxies (e.g. Davies et al. 1993; Trager et al. 2000b; Davies et al. 2001; Thomas et al. 2005; Kuntschner et al. 2002a). In subsequent papers of this series we will compare the index measurements of globular clusters with indices derived from our long-slit spectra of the hosts' diffuse stellar light.

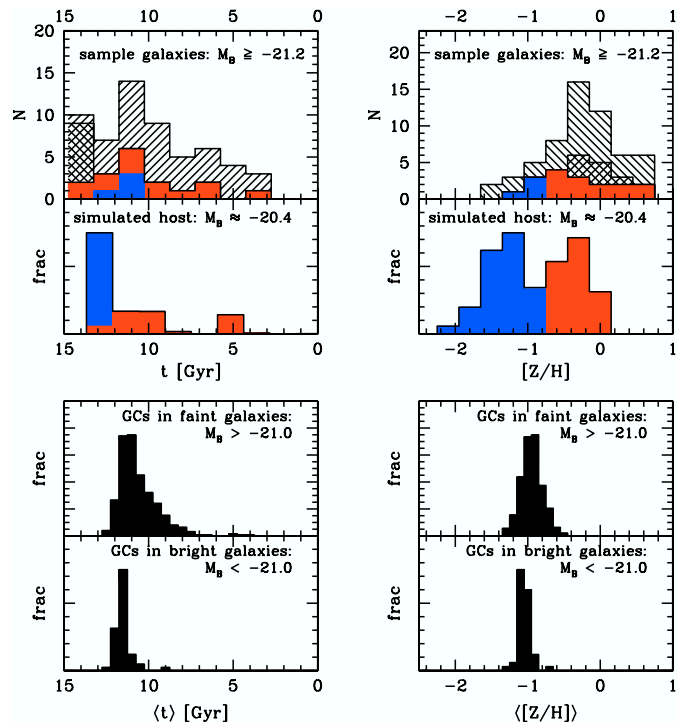In the following we summarize the major findings of this section:

- globular clusters in early-type galaxies have on average super-solar [α/Fe] ratios with a mean ~0.45 dex;
- metal-rich globular clusters have on average lower [α/Fe] ratios than their metal-poor counterparts;
- young and old globular clusters have on average similar [α/Fe] ratios.

6. Discussion

6.1. Assembly history of early-type galaxies

If the dispersion in Balmer-[MgFe]′ diagnostic plots is entirely driven by age[7], we find indications for a significant fraction of relatively young globular clusters in early-type galaxies. About ~1/3 of our sample globular clusters have formal ages younger than 10 Gyr, implying formation redshifts $z_f \lesssim 1.7$ (in a ΛCDM *concordance* universe).

In Fig. 8 we compare the derived ages and metallicities of our high-quality sample with the corresponding distributions of globular cluster systems simulated according to a hierarchical

---

[7] A population of warm horizontal branch stars remains a potential cause for increased Balmer line strengths.

Fig. 8. *Top row*: comparison of globular cluster ages and metallicities in our sample galaxies with those in a simulated host galaxy with a similar luminosity (mass). All globular cluster in our sample are shown as hatched histograms, outliers in diagnostic plots are indicated by double-hatched histograms (see Sect. 4.2), and high-quality data is shown as solid histograms. Observed and simulated globular cluster samples were split into metal-poor and metal-rich globular clusters at [Z/H] = −0.9 and the shading is accordingly transferred to the age distribution plot. *Bottom row*: average ages and metallicities of simulated globular cluster systems in faint and bright host galaxies. All predictions were taken from Beasley et al. (2002a).

merging scenario (Beasley et al. 2002a). As the average luminosity of our sample host galaxies is $\langle M_B \rangle_{sample} = -20.4 \pm 0.6$ (see Table 1), we use the globular cluster system of a typical simulated galaxy with a similar luminosity $M_B = -20.42$ (see also Fig. 6 in Beasley et al. 2002a) for comparison. We split both cluster samples (simulated and observed) in metal-poor and metal-rich clusters at [Z/H] = −0.9. The top right panel of Fig. 8 shows that our sample is biased towards metal-rich globular clusters, and the comparison of metal-poor globular clusters is limited to the statement that both observed and simulated clusters are all consistently old. For metal-rich globular clusters there is good agreement in the age range covered by data and simulations.

The somewhat naive prediction of more extended formation timescales of more massive structures in the hierarchical picture holds only if the fraction of gas-poor to gas-rich mergers, the so-called dry to mixed merger ratio, is constant with redshift. Khochfar & Burkert (2003) predict that this ratio depends on galaxy mass in the sense that most massive ellipticals formed early in rather dissipationless (dry) mergers of bulge-dominated precursors (see also Kauffmann & Haehnelt 2000). This would imply that on average low-luminosity

ellipticals would harbor a higher fraction of young globular clusters, while most massive galaxies would preferentially host old globular cluster systems. This is reflected in the simulations of Beasley et al. (2002a). The lower panels of Fig. 8 illustrate the mean ages and metallicities of globular cluster systems in faint and bright galaxies with a cut at $M_B = -21.0$. The plots show that while host galaxy luminosity affects the mean metallicity of globular cluster systems only marginally, a significant fraction ($\sim$25%) of low-luminosity galaxies is predicted to host globular cluster systems with an average age younger than $\sim$10 Gyr, compared to a tiny fraction ($\sim$2%) in bright galaxies. Unfortunately, the transition between dry and mixed merger-dominated evolution is predicted to occur for early-type galaxies in the luminosity range between $M_B \approx -20$ and -21 mag, where all of our sample galaxies reside.

To first order, previous spectroscopic studies find evidence for mostly old globular cluster systems in the massive Fornax galaxy NGC 1399 (Kissler-Patig et al. 1998), and the two Virgo galaxies M 87 (Cohen et al. 1998) and M 49 (Cohen et al. 2003), which appears to fit into the framework of *dissipationless* merging with an early assembly. We will get back to this point in a subsequent paper in which globular cluster systems will be investigated as a function of the host galaxy property.

6.2. Formation timescales

Stellar populations with super-solar [α/Fe] ratios, as they are observed in massive elliptical galaxies, are generally interpreted as the result of very short formation time scales. However, in the case of dissipative merging, hierarchical merging models predict frequent merging events, which is expected to result in relatively low [α/Fe] ratios (e.g. Thomas et al. 1999). Although somewhat on the high side, our formal mean [α/Fe] ratio of $\sim$0.47 dex for globular clusters in early-type galaxies is in line with values measured for the diffuse light. Hence, the formation time scales of field stars and globular clusters appear to be similar in elliptical galaxies and not immediately compatible with hierarchical merging models.

The found evidence for a [α/Fe]–metallicity relation in early-type globular cluster systems is consistent with a generic chemical enrichment scenario in which more metal-rich stellar populations have lower α-element enhancements. Two types of supernovae contribute to the build-up of α-peak (type II) and iron-peak elements (type Ia) in the interstellar medium on different time scales (e.g. Matteucci 1994; Thomas et al. 1999), because of the evolutionary delay of $\sim$1 Gyr of type-Ia supernova progenitors (Greggio 1997). Since globular clusters are not massive enough to support significant self-enrichment, their [α/Fe] ratios reflect the *large-scale* chemical conditions during their formation. However, to allow a detectable increase in [α/Fe], for high-metallicity stellar populations it requires a larger number of type II supernovae to outweigh any previous metal-enrichment by type Ia supernovae compared to lower metallicities. This implies that high [α/Fe] ratios at high metallicities are likely the result of *shorter* formation timescales and/or higher star-formation rates than similar [α/Fe] ratios at lower metallicities. Careful modeling of the chemical

evolution of a globular cluster system is needed to quantify these formation timescales. The relation between [α/Fe] and metallicity found here provides the first important constraint for this exercise.

It is also important to test whether a steeper [α/Fe]–age relation can be found for globular cluster systems in more massive galaxies, which would be expected if these systems formed on more extended timescales, as predicted by hierarchical merging models.

7. Summary and conclusions

We have conducted a study of ages, metallicities, and [α/Fe] ratios of extragalactic globular clusters in early-type galaxies, based on the Lick index system. We find that up to $\sim$1/3 of our sample of globular clusters have ages formally younger than 10 Gyr. This result is not biased by one single globular cluster system in our galaxy sample and appears representative for early-type galaxies in general. We cannot state with confidence whether the younger ages (i.e. $t < 10$ Gyr) are real or due to an unexpected blue horizontal branch morphology at high metallicities. If the younger ages are real, the found fraction should be taken as an upper limit, since our data only probe the bright end of the globular cluster luminosity function where relatively young globular clusters, if present, are expected to reside. In general, less than $\sim$1/3 of the brightest $\sim$10% of globular cluster systems in early-type galaxies which we sample with our study could have formed at redshifts $z_f \lesssim 1.7$.

We find that the formal age scatter increases and the mean age decreases from metal-poor to metal-rich globular clusters, resulting in an age–metallicity relation. For our high-quality sample globular clusters with metallicities [Z/H] < -0.6 we find an age dispersion of 0.5 Gyr. The metal-rich sub-sample has a dispersion of 3.5 Gyr.

Our high-quality sample spans a wide range in metallicity between [Z/H] ≈ -1.3 and $\sim$+0.5 dex. We find evidence for an [α/Fe]–metallicity relation in the sense that more metal-rich globular clusters have lower α-element enhancements, which needs to be confirmed with more data that better sample the metal-poor regime. However, there is no indication for an [α/Fe]–age correlation.

[α/Fe] ratios are found to be on average super-solar with a mean 0.47 ± 0.06 dex and a dispersion of $\sim$0.3 dex, which indicates formation timescales shorter than $\sim$1 Gyr. In other words, the progenitor clouds of globular clusters were predominantly enriched by type-II SNe.

References

Arimoto, N., & Yoshii, Y. 1987, A&A, 173, 23

Ashman, K. M., & Zepf, S. E. 1998, Globular Cluster Systems (Cambridge University Press)

Barmby, P., Huchra, J. P., Brodie, J. P., et al. 2000, AJ, 119, 727

Baugh, C. M., Cole, S., Frenk, C. S., & Lacey, C. G. 1998, ApJ, 498, 504

Beasley, M. A., Baugh, C. M., Forbes, D. A., Sharples, R. M., & Frenk, C. S. 2002a, MNRAS, 333, 383

Beasley, M. A., Hoyle, F., & Sharples, R. M. 2002b, MNRAS, 336, 168

Beasley, M. A., Brodie, J. P., Strader, J., et al. 2004, AJ, 128, 1623

Bender, R. 1988, A&A, 202, L5

Bender, R. 1996, New Light on Galaxy Evolution, IAU Symp., 171, 181

Bender, R., Ziegler, B., & Bruzual, G. 1996, ApJ, 463, L51

Bower, R. G., Lucey, J. R., & Ellis, R. S. 1992, MNRAS, 254, 601

Burstein, D., Faber, S. M., Gaskell, C. M., & Krumm, N. 1984, ApJ, 287, 586

Burstein, D., Li, Y., Freeman, K. C., et al. 2004, ApJ, 614, 158

Caldwell, N. 1984, PASP, 96, 287

Charlot, S., Worthey, G., & Bressan, A. 1996, ApJ, 457, 625

Cohen, J. G., Blakeslee, J. P., & Ryzhov, A. 1998, ApJ, 496, 808

Cohen, J. G., Blakeslee, J. P., & Côté, P. 2003, ApJ, 592, 866

Cole, S., Lacey, C. G., Baugh, C. M., & Frenk, C. S. 2000, MNRAS, 319, 168

Davies, R. L., Sadler, E. M., & Peletier, R. F. 1993, MNRAS, 262, 650

Davies, R. L., Kuntschner, H., Emsellem, E., et al. 2001, ApJ, 548, L33

Elson, R. A. W. 1997, MNRAS, 286, 771

Faber, S. M. 1972, A&A, 20, 361

Forbes, D. A., Brodie, J. P., & Larsen, S. 2001, ApJ, 556, L83

Franx, M., & Illingworth, G. D. 1988, ApJ, 327, L55

de Freitas Pacheco, J. A., & Barbuy, B. 1995, A&A, 302, 718

González, J. J. 1993, Ph.D. Thesis, University of California, Santa Cruz

Goudfrooij, P., & Emsellem, E. 1996, A&A, 306, L45

Goudfrooij, P., Hansen, L., Jorgensen, H. E., & Norgaard-Nielsen, H. U. 1994, A&AS, 105, 341

Goudfrooij, P., Alonso, M. V., Maraston, C., & Minniti, D. 2001, MNRAS, 328, 237

Goudfrooij, P., Strader, J., Brenneman, L., et al. 2003, MNRAS, 343, 665

Gregg, M. D., Ferguson, H. C., Minniti, D., Tanvir, N., & Catchpole, R. 2004, AJ, 127, 1441

Greggio, L. 1997, MNRAS, 285, 151

Greggio, L., & Renzini, A. 1990, ApJ, 364, 35

Grillmair, C. J., Lauer, T. R., Worthey, G., et al. 1996, AJ, 112, 1975

Harris, W. E. 1996, AJ, 112, 1487, for the 1999 update see http://physun.physics.mcmaster.ca/~harris/mwgc.dat

Harris, W. E. 2001, Star Clusters, 223

Harris, W. E., & van den Bergh, S. 1981, AJ, 86, 1627

Harris, W. E., & Harris, G. L. H. 2002, AJ, 123, 3108

Homeier, N., Gallagher, J. S., & Pasquali, A. 2002, A&A, 391, 857

Ibata, R. A., Gilmore, G., & Irwin, M. J. 1995, MNRAS, 277, 781

Jedrzejewski, R., & Schechter, P. L. 1988, ApJ, 330, L87

Johnson, K. E., Vacca, W. D., Leitherer, C., Conti, P. S., & Lipscy, S. J. 1999, AJ, 117, 1708

Kauffmann, G., White, S. D. M., & Guiderdoni, B. 1993, MNRAS, 264, 201

Kauffmann, G., & Haehnelt, M. 2000, MNRAS, 311, 576

Kissler-Patig, M., Richtler, T., Storm, J., & della Valle, M. 1997, A&A, 327, 503

Kissler-Patig, M., Brodie, J. P., Schroder, L. L., et al. 1998, AJ, 115, 105

Khochfar, S., & Burkert, A. 2003, ApJL, 597, 117

Koo, D. C., Vogt, N. P., Phillips, A. C., et al. 1996, ApJ, 469, 535

Korn, A., Maraston, C., & Thomas, D. 2005, A&A, submitted

Kuntschner, H. 2000, MNRAS, 315, 184

Kuntschner, H., Smith, R. J., Colless, M., et al. 2002a, MNRAS, 337, 172

Kuntschner, H., Ziegler, B. L., Sharples, R. M., Worthey, G., & Fricke, K. J. 2002b, A&A, 395, 761

Larsen, S. S., & Richtler, T. 2000, A&A, 354, 836

Larsen, S. S., Brodie, J. P., Beasley, M. A., & Forbes, D. A. 2002, AJ, 124, 828

Larsen, S. S., Brodie, J. P., Beasley, M. A., et al. 2003, ApJ, 585, 767

Larson, R. B. 1975, MNRAS, 173, 671

Lee, Y., Demarque, P., & Zinn, R. 1994, ApJ, 423, 248

Lee, H., Yoon, S., & Lee, Y. 2000, AJ, 120, 998

Macchetto, F., Pastoriza, M., Caon, N., et al. 1996, A&AS, 120, 463

Maraston, C. 1998, MNRAS, 300, 872

Maraston, C. 2003, Extragalactic Globular Cluster Systems, Proceedings of the ESO Workshop held in Garching, Germany, 27–30 August 2002, 237

Maraston, C. 2005, MNRAS, accepted [arXiv:astro-ph/0410207]

Maraston, C., & Thomas, D. 2000, ApJ, 541, 126

Maraston, C., Greggio, L., Renzini, A., et al. 2003, A&A, 400, 823

Matteucci, F. 1994, A&A, 288, 57

McLaughlin, D. E. 1999, AJ, 117, 2398

O'Connell, R. W. 1976, ApJ, 206, 370

Osterbrook, D. E. 1989, Astrophysics of Gaseous Nebulae and Active Galactic Nuclei (Mill Valley: University Science Books)

Peebles, P. J. E. 2002, in A New Era in Cosmology, ed. N. Metcalfe, & T. Shanks, ASP Conf. Ser., in press

Phillips, M. M., Jenkins, C. R., Dopita, M. A., Sadler, E. M., & Binette, L. 1986, AJ, 91, 1062

Poggianti, B. M., Bridges, T. J., Carter, D., et al. 2001, ApJ, 563, 118

Puzia, T. H., Kissler-Patig, M., Brodie, J. P., & Huchra, J. P. 2000, AJ, 120, 777

Puzia, T. H., Saglia, R. P., Kissler-Patig, M., et al. 2002, A&A, 395, 45

Puzia, T. H., Kissler-Patig, M., Thomas, D., et al. 2004, A&A, 415, 123 (Paper I)

Puzia, T. H., Perrett, K. M., & Bridges, T. J. 2005, A&A, 434, 909

Reader, J., & Corliss, Ch. H. 1981, CRC Handbook of Chemistry and Physics

Rich, R. M., Sosin, C., Djorgovski, S., et al. 1997, ApJ, 484, L25

Rich, R. M., et al. 2003, AJ, in press

Rosen, B. 1952, Constantes sélectionnées ; atlas des longueurs d'onde caractéristiques des bandes d'émission et d'absorption des molécules diatomiques (Paris : Hermann & Cie, Dépositaires)

Schweizer, F. 1997, The Nature of Elliptical Galaxies; 2nd Stromlo Symposium, ASP Conf. Ser., 116, 447

Silk, J. 1977, ApJ, 214, 152

Somerville, R. S., Primack, J. R., & Faber, S. M. 2001, MNRAS, 320, 504

Surma, P., & Bender, R. 1995, A&A, 298, 405

Thomas, D., Greggio, L., & Bender, R. 1999, MNRAS, 302, 537

Thomas, D., Maraston, C., & Bender, R. 2003, MNRAS, 339, 897

Thomas, D., Maraston, C., & Korn, A. 2004, MNRAS, 351, L19

Thomas, D., Maraston, C., Bender, R., & de Oliveira, C. M. 2005, ApJ, 621, 673

Tinsley, B. M. 1972, ApJ, 178, 319

Tinsley, B. M. 1979, ApJ, 229, 1046

Tonry, J. L., Dressler, A., Blakeslee, J. P., et al. 2001, ApJ, 546, 681

Trager, S. C., Worthey, G., Faber, S. M., Burstein, D., & Gonzalez, J. J. 1998, ApJS, 116, 1

Trager, S. C., Faber, S. M., Worthey, G., & González, J. J. 2000a, AJ, 119, 1645

Trager, S. C., Faber, S. M., Worthey, G., & González, J. J. 2000b, AJ, 120, 165

Treu, T., Stiavelli, M., Casertano, S., Møller, P., & Bertin, G. 1999, MNRAS, 308, 1037

Tripicco, M. J., & Bell, R. A. 1995, AJ, 110, 3035

Tully, R. B. 1988, Nearby Galaxy Catalog (Cambridge and New York: Cambridge University Press)

de Vaucouleurs, G., de Vaucouleurs, A., Corwin, H. G., Jr., et al. 1991, Third Reference Catalogue of bright galaxies (Berlin: Springer)

White, S. D. M., & Rees, M. J. 1978, MNRAS, 183, 341

Whitmore, B. C., & Schweizer, F. 1995, AJ, 109, 960

Worthey, G. 1994, ApJS, 95, 107

Worthey, G., & Ottaviani, D. L. 1997, ApJS, 111, 377

Worthey, G., Faber, S. M., Gonzalez, J. J., & Burstein, D. 1994, ApJS, 94, 687